RSC Advances

PAPER

Cite this: *RSC Adv.*, 2016, **6**, 103872

On-chip electrical detection of parallel loop-mediated isothermal amplification with DG-BioFETs for the detection of foodborne bacterial pathogens†

Carlos Duarte-Guevara,[ab] Vikhram V. Swaminathan,[b] Bobby Reddy, Jr.,[b] Jui-Cheng Huang,[c] Yi-Shao Liu[d] and Rashid Bashir*[e]

The use of field effect transistors (FETs) as the transduction element for the detection of DNA amplification reactions will enable portable and inexpensive nucleic acid analysis. Transistors used as biological sensors, or BioFETs, minimize the cost and size of detection platforms by leveraging fabrication methods already well developed for electronics. Here, we report a dual-gate BioFET (DG-BioFET) array platform with 1024×1024 sensors that is used for on-chip electrical detection of loop-mediated isothermal amplification (LAMP) reactions that target food borne bacterial pathogens. The DG-BioFETs of our 7 × 7 mm^2 array are able to electrically detect pH changes that are triggered by nucleotide incorporation during LAMP elongation. Multiple 250 nL reactions can be simultaneously electrically monitored in our array that is divided in 30 micro-chambers with gold-coated anisotropically etched silicon wells that act both as reference electrode and confinement element. Our characterization results show that the gold-biased DG-BioFETs have a sensitivity of 32 mV pH^{-1} (equivalent to 2 μA pH^{-1}) and an average resolution of 0.5 pH units. This sensitivity is high enough to detect the pH changes triggered by the amplification reaction, but to maximize our signal-to-noise ratio and improve our quantitative conclusions we use a group of data analysis techniques that are available in our high-density platform that monitors each reaction with ∼3500 independent BioFETs. We use redundancy techniques to minimize the overall standard deviation of our measurements, the Grubbs test to eliminate measurements outside the expected normal distribution, and reference micro-chambers to subtract the common noise. With these techniques we are capable of reducing the *P* value, of a *t*-test comparing positive and negative readings, from a typical 0.17 to 0.03. The platform that we present along with the analysis techniques that we developed allow the on-chip electrical detection and identification of *E. coli* O157 and *S. typhi* with parallel LAMP assays targeting eae and invA genes. The LAMP reactions are highly specific, without false positives, and our titration assays demonstrate a limit of detection of 23 CFU per reaction on chip.

Received 4th August 2016
Accepted 19th October 2016

DOI: 10.1039/c6ra19685c

www.rsc.org/advances

Introduction

In the past few decades the food safety industry has achieved important milestones to improve the quality of products and control over the production chain.[1] New biomolecular assays have been included in pathogen screening protocols enhancing the response time, sensitivity, and accuracy of detection protocols.[2–4] Also, better understanding of the behavior of pathogenic entities has resulted in updated handling procedures that further reduce risk of contamination.[5] However, despite these important advances, food safety is still one of the major concerns in the developed and underdeveloped world.[6] During 2013 FoodNet (http://www.cdc.gov/foodnet/index.html) reported more than 19 000 cases of confirmed foodborne infections that resulted in 4200 hospitalizations and 80 deaths in the United States. It is estimated that foodborne illness represents an annual economic burden of $78 billion dollars[7] and contamination outbreaks severely damage the economic viability of companies and consumer trust.[8,9] The situation is aggravated by two important factors, a mutating enemy and a more intricate food production system. Large recent outbreaks,

[a]*Department of Electrical and Computer Engineering, University of Illinois at Urbana-Champaign, Urbana, IL 61801, USA*
[b]*Micro and Nanotechnology Laboratory, University of Illinois at Urbana-Champaign, Urbana, IL 61801, USA*
[c]*Design and Technology Platform, Taiwan Semiconductor Manufacturing Company, Hsinchu, Taiwan*
[d]*Research and Ecosystem, Delta Electronics Inc., 417939 Singapore*
[e]*Department of Bioengineering, University of Illinois at Urbana-Champaign, Urbana, IL 61802, USA. E-mail: rbashir@Illinois.edu*

† Electronic supplementary information (ESI) available. See DOI: 10.1039/c6ra19685c

like the 2011 *E. coli* O104:H4 HUS epidemic in Germany, demonstrated that microorganisms previously catalogued as non-adulterants can cause serious illness, and that rapid mutation of bacterial serotypes turn harmless into pathogenic species.[10] Additionally, in a more connected economy, diversity and complexity of food products makes it difficult to enforce regulations.[11] Imports of agricultural goods have doubled in the last decade and the assembly of products with raw materials from multiple locations complicates analysis, tracing, and other food safety controls.[12] To prevent foodborne related infections under these challenging and evolving conditions, it is necessary to create new tools and practices that can meet public health goals.[13]

One of the fundamental disadvantages of the current food regulation and protection system is that it is based on central laboratories where samples are shipped for analysis. The transportation of food samples from production or packaging sites to laboratories for analysis is expensive.[14] Moving samples between different sites requires the development of transport infrastructure, handling procedures, and packaging protocols that augment the cost of the screening assay and significantly increase the time to result.[15] Therefore, in the centralized screening laboratory model, samples are infrequently tested with troubling estimates indicating that only 2% of all the imported food products are inspected for contamination.[16,17] An ideal solution, enabled by the novel combination of microfabrication techniques and novel biomolecular assays, is to create the equivalent of 'point-of-care' systems that can detect pathogenic presence on-site, in a simple assay performed by untrained personnel.[15,18] Researchers have been actively pursuing better tools for the detection of pathogens employing multiple methodologies that aim to minimize the footprint and complexity of the detection devices. For example, microfluidic impedance spectroscopy has been used to detect specific pathogen growth when it is combined with capture antibodies,[19] bioluminescent phages were developed to easily detect metabolic activity of target microorganisms,[20] and lateral flow assays are used for inexpensive detection with disposable sensors.[21] These proposed pathogen detection methods aim to substitute standards, but the preferred approach is still the identification and detection of foodborne pathogens through nucleic acid amplification.[22]

DNA-based pathogen screening

DNA-based methods for microorganism detection provide unchallenged specificity, sensitivity, and robustness. Nowadays these methods are extensively used as screening assays prior to culture confirmations. In fact, polymerase chain reaction (PCR) assays have been incorporated in the Food Safety and Inspection Service (USDA-FSIS) manuals for pathogen detection and are routinely used as the first indicator of contamination.[4] Therefore, a popular approach to improve the instrumentation for the detection of pathogens is to reduce cost and complexity of DNA amplification assays by developing portable systems for nucleic acid detection. Relevant examples include: 'Gene-Z' that uses a microfluidic chip to partition a liquid sample and fluorescently detect loop mediated isothermal amplification (LAMP) reactions,[23] 'FilmArray' that has developed a gastrointestinal panel of nested PCR for automated and multiplexed detection of pathogenic entities,[24] or compact disk inspired devices that simplify arraying of samples and reaction preparation with ubiquitous and inexpensive tools.[25] Additionally, novel miniaturized systems integrate giant magnetoresistance with line probe assays to perform parallel LAMP.[26] The incorporation of magnetic nanoclusters labeled with streptavidin to the LAMP reaction enables the electrical detection of the amplification reaction. These strategies demonstrate that DNA amplification reactions can be performed in multiple setups by minimizing the footprint of equipment and simplifying preparatory steps. Unfortunately, these new systems for DNA amplification detection have not been successfully incorporated into pathogen screening protocols due to high cost per test, poor robustness, or the complexity of reading stations. Other systems require additional reagents and labeling agents that augment the test reaction cost and complexity. Hence, new systems that meet the food safety requirements of very large and frequent testing are currently being studied to improve the regulator's ability to detect and control contamination.

An emerging approach for portable detection of DNA amplification reactions leverages advances in the semiconductor industry to minimize cost and size of detection tools while enhancing their robustness and level of automation.[27] After more than 50 years of exponential improvements, the semiconductor industry nowadays can easily fabricate transistors at fractions of a penny and pack millions in a microscopic area.[28] This ability in combination with recent research on ionic and molecular sensing with field effect transistors has created a pathway to incorporate semiconductor devices in bio-sensing applications.[29] The use of inexpensive and highly dense transistor chips has already demonstrated that can minimize the cost and size of DNA sequencing tools[30] or point-of-care devices,[31] and similar approaches will yield novel biosensing systems for food safety. In this paper, we describe the parallel detection of foodborne pathogens through LAMP reactions detected with a dense dual-gated biological field effect transistor (DG-BioFET) array of 1024×1024 sensors distributed in 7 × 7 mm^2. Fig. 1(a) shows the DG-BioFET array divided in several independent micro-chambers. Each chamber is defined by anisotropically etched gold-coated silicon wells that are bonded to the sensing area with a PDMS layer. The gold-coated silicon acts both as the confinement element, to create independent reactions in our limited area, and a pseudo-reference electrode to bias the electrolyte and gate the transistors. With this setup, BioFETs monitor up to 30 independent 250 nL reactions electrically recognizing pH changes triggered by LAMP reactions that target specific genes determined by dehydrated primers.[32] When the dehydrated primers match the template in solution, the incorporation of nucleotides during LAMP releases hydrogen ions and changes the solution's acidity. Therefore, the pH of the solution can be monitored to detect the amplification reaction. This 'pH-LAMP' reactions provide a potentiometric and label-free detection of the amplification reaction that is ideally suited for miniaturized systems.[33] In each reaction chamber we

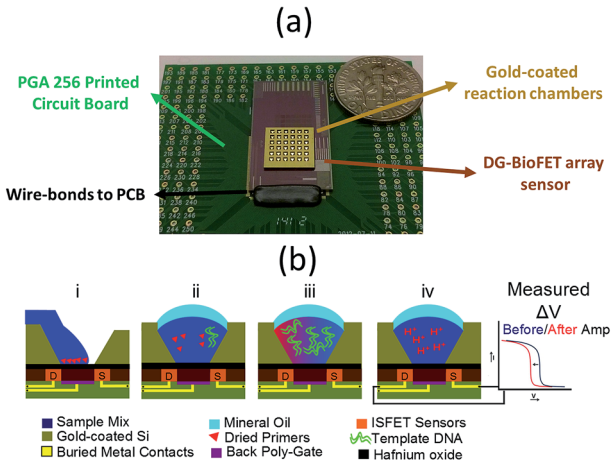

Fig. 1 Photograph and detection assay schematics. (a) Photograph of the assembled sensor highlighting the semiconductor chip, goal-coated reaction chambers, and connections to PCB. (b) Brief description of the pathogen detection protocol with: (i) primer dehydration and sample injection, (ii) primer resuspension and annealing to target sequence, (iii) DNA amplification, and (iv) electrical detection of pH changes.

perform miniaturized detection assays, previously developed and confirmed,[34,35] in a simple protocol that is briefly summarized in the schematic of Fig. 1(b). In the following sections we describe our experimental setup and protocol, present characterization results of our sensing platform, and demonstrate the electrical detection of LAMP reactions. Even though the pH changes related to amplification only provide small electrical signals it is possible to obtain statistically significant results when data analysis techniques are used to improve the signal-to-noise ratio. Our unique platform, with over a million BioFET sensors, allows us to utilize redundancy, elimination, and subtraction techniques to clear the recorded signal, improve our quantification, and statistically demonstrate the ability of the BioFETs to detect the ions released from LAMP reactions without the added reagents or labeling agents. Finally, we employ these different methods to show the parallel electrical detection of *Escherichia coli* O157 and *Salmonella typhimurium*. Using the assays previously developed by Ge *et al.* in conjunction with our DG-BioFET platform and data analysis techniques, we demonstrate specific on-chip electrical detection of LAMP reactions and evaluate the system's limit of detection.

Experimental section

Dual-gate BioFET array fabrication

The DG-BioFET array is fabricated in collaboration with Taiwan Semiconductor Manufacturing Company (TSMC) with a CMOS compatible process that has been described earlier.[36] Briefly, the process starts with the fabrication of standard metal–oxide–semiconductor (MOS) devices in a silicon-on-insulator (SOI) wafer. The device layer of the SOI is then bonded to a carrier wafer and the SOI's bulk silicon its CMP etched revealing the buried oxide. A lithography and dry-etch step is then used to selectively remove the buried oxide from sensing areas and a hafnium oxide layer is deposited to act as the gate dielectric of DG-BioFETs. Hence, the BioFETs have a bottom MOS gate and a high-k fluid gate. A schematic cross-section of one DG-BioFET sensor is presented in Fig. S1.† In addition, the layout of initial MOS devices includes decoding circuits for row and column addressing enabling the serial read-out of all the sensor's drain current. The finalized chip is mounted in a 256 pin printed circuit board (PCB) with wire-bonds connecting the chip contact pads to the PCB.

Gold-coated chambers to bias micro-droplets in the array

In order to monitor multiple isolated reactions in our BioFET array it is necessary to have a method to electrically bias each micro-droplet. A common strategy is to create on-chip pseudo-reference electrodes that are patterned on the array.[37,38] We attempted to use this approach for droplet biasing and patterned gold electrodes in our sensing area. An image of the chip with patterned gold pseudo-reference electrodes is presented in Fig. S2(a).† However, this approach has three important drawbacks that motivated our search for alternative methods. First, the fabrication of these electrodes in our foundry fabricated chips is complex and expensive. The deposition of precious metals on the device has to be carried out outside the production line and it requires multiple exchanges between vendors before the device is wire-bonded significantly adding cost and fabrication time. Second, the lift-off process affects the transconductance of the devices. In Fig. S2(b)† we present a drain current heat-map of the array with on-chip electrodes when biased with the fluid-gate. It shows low currents in the exposed devices, suggesting lower response to surface potential changes and a consequent lower sensitivity. Finally, placing droplets on the array was challenging with on-chip electrodes. Positioning droplets on a flat surface with electrodes requires a very precise spotting system, limits the volume of each reaction, and reduces the density of reactions. In addition, the hydrophilicity ratios between metal and oxide complicates droplet placement in the sensing BioFETs. As it is shown in Fig. S2(c),† the reaction droplets tend to align with the metal electrodes reducing the sensors that are directly monitoring the reaction. Therefore, after discarding on-chip electrodes as a method of droplet biasing, we found a simple solution in the gold-coated micro-chambers. Gold-coated chambers partition the BioFET array and create multiple wells for parallel LAMP detection while creating a single node pseudo-reference electrode. These chambers can be bonded to the chip after wire-bonding, do not affect the device performance, enables reactions with larger volumes, and simplify the droplets placement.

The fabrication of the gold-coated chambers is done with a standard silicon wafer (University Wafers, Boston, MA) that is thinned down with cycles of oxidation and hydrofluoric etch to achieve a thickness of ~200 μm. The wafer is left with 80 nm of silicon oxide to create a hard mask, done with standard SPR220 photolithography (MicroChem, Westboroguh, MA) and 10 : 1 BOE etch (Avantor, Center Valley, PA), which defines the silicon that will be etched to form the micro-chambers. Silicon not

protected by the SiO_2 mask is anisotropically carved through the wafer in a 1 : 1 TMAH (Sigma-Aldrich, St. Louis, MO) bath for 36 h at 80 °C, creating an array of chambers. After TMAH etching, 20 nm of Ti and 80 nm of Au are deposited on the wafer with an E-beam evaporator (CHA Industries, Freemont, CA). With this metallic coating, the wells are not only the confinement element of the reaction but will also be a pseudo-reference electrode.[39–41] Finally, a layer of uncured Sylgard PDMS (Dow Corning, Midland, MI) is spin coated in the back of diced gold-coated chips that are then bonded to the 7 × 7 mm^2 DG-BioFET sensing area and baked at 60 °C for 3 h. The resulting sensing chip is presented in Fig. 1(a).

Testing setup

The assembled chip is connected to a customized PCB with a 256 PGA socket that sets inputs and outputs connections with a PXI logic IC tester (OpenATE, Hsinchu, Taiwan). The IC tester excites the decoding circuit to select sensors, sets biasing conditions for FET operation, and records the output of a *trans*-impedance amplifier that magnifies the BioFETs drain current. The process is coordinated with custom-built software that outputs a 2D array of the recorded currents. In addition, the circuitry in the testing setup is designed to have an external contact with the fluid-gate biasing voltage. This node is directed to a micromanipulator probe (Micromanipulator, Carson City, NV) that is put in contact with the deposited gold on the silicon wells to bias the electrolytes of all the reaction chambers with a single fluid-gate voltage. All elements of the measurement setup are shown in Fig. S3.†

pH sensitivity measurements

The pH of 10 mM phosphate buffered saline (PBS) is modified by diluting hydrochloric acid and sodium hydroxide until a desired pH calibration value is obtained. Solutions are adjusted with an Orion 3 start pH meter (Thermo Scientific, Pittsburgh, PA) and injected into the reaction chambers with a micro-injector IM-300 (Narishige Scientific Instrument Lab., Tokyo, JP). With the droplets of the calibration pH solution inside the micro-chambers, the chip is connected to the testing station, the gold is biased to the desired fluid-gate potential with the micromanipulator, and the drain current of each BioFET in the array is recorded. Subsequent measurements are obtained by swapping the PBS solution for one with a different pH. Electrolyte acidity induced current changes are correlated with surface charge in the hafnium oxide layer indicating the surface potential sensitivity to pH changes.

LAMP reaction

LAMP protocols and primers for the detection of pathogenic genes of *E. coli* and *S. typhi* are taken from prior publications by Ge *et al.*[34,35] For the on-chip operation the amplification assay is divided in 3 different stages: chip preparation, electrical profiling prior to the reaction, and measurements after the reaction. In the chip preparation stage, 30 nL of primer mix for the selected pathogen is dispensed and air-dried inside the micro-chambers. The sequences of LAMP primers for the amplification of eae (*E. coli*) and invA (*S. typhi*) are specified in Table 1. They are prepared from customized oligos (iDT DNA, Coralville, IA) at concentrations of 19 μM for FIP/BIP pair, 9.6 μM for loop primers LF/LB, and 2.4 μM for F3/B3. After the primers are dehydrated, a primer-less LAMP reaction mix, which has been optimized to trigger pH changes,[38] is injected in all the reaction chambers. The LAMP reaction mix consisted of 0.1× Isothermal amplification buffer, 1.3 mM of dNTP mix, 5 mM of magnesium sulfate, 6 units of Warmstart Bst 2.0 polymerase (all four from New England Biolobs, Ipswich, MA), 800 mM Betaine, 55 mM KCl (both from Sigma-Aldrich), 1× EvaGreen (Biotium, Hayward, CA), and template DNA. The DNA is extracted from bacterial cultures, *E. coli* O157:H7 in brain-heart infusion medium or *S. typhi* in Lysogeny broth (Fisher Scientific, Pittsburgh, PA), and growth overnight in a 34 °C incubator. For DNA extraction, bacterial cells in media are centrifuged at 8600 rcf for 3 min and re-suspended in DI water, lysed at 95 °C for 15 min, and centrifuged again (12 500 rcf for 10 min) to remove cell debris, leaving template DNA in the supernatant. With this protocol, the extracted DNA concentrations from carrying capacity cultures of *E. coli* and *S. typhi* are estimated at 85.1 ± 4.7 and 35.9 ± 7.1 ng μL^{-1}. The ND-1000 spectrophotometer (NanoDrop, Wilmington, DE) results are presented in Fig. S4.†

In the second stage of the detection protocol, the primer-less LAMP solution is microinjected in the reaction chambers and immediately covered with mineral oil to prevent evaporation during the heating stages. After injection, the fluorescence intensity of the reaction chambers is obtained with a Nikon Eclipse FN-1 microscope (Nikon Instruments Inc. Melville, NY) and electrical characteristics of BioFETs are obtained with the IC tester, obtaining optical and electrical measurements prior the amplification reactions. The chip is then taken to an oven at 60 °C to trigger LAMP reactions.

Finally, after the chip is heated up in a convection Isotemp oven (Fisher Scientific) to 60 °C for 60 min, the fluorescence intensity and electrical characteristics are measured again. Differences between before/after states and differential signals

Table 1 LAMP primers used in this study targeting eae gene for the detection of *E. coli* O157 and invA for the detection of *S. typhi*

Target gene	Primer sequence	Source
eae	F3 TGACTAAAATGTCCCCGG	34
	B3 CGTTCCATAATGTTGTAACCAG	
	FIP GAAGCTGGCTACCGAGACTC-CCAAAAGCAACATGACCGA	
	BIP GCGATCTCTGAACGGCGATT-CCTGCAACTGTGACGAAG	
	LF GCCGCATAATTTAATGCCTTGTCA	
	LB ACGCGAAAGATACCGCTCT	
invA	F3 CGGCCCGATTTTCTCTGG	35
	B3 CGGCAATAGCGTCACCTT	
	FIP GCGCGGCATCCGCATCAATA-TGCCCGGTAAACAGATGAGT	
	BIP GCGAACGGCGAAGCGTACTG-TCGCACCGTCAAAGGAAC	
	LF GGCCTTCAAATCGGCATCAAT	
	LB GAAAGGGAAAGCCAGCTTTACG	

against negative controls will reveal DNA amplification products in chambers where the primer set, dehydrated in the preparation stage, finds a matching template. Therefore, positive reactions will indicate the presence of the target pathogen in the sample. The amplification and measurement steps are briefly described in the schematic of Fig. 1(b).

The fluorescence images acquired of the micro-chambers before and after the reaction are analyzed with ImageJ. Droplets expand and change shape during the reaction due to byproducts, such as pyrophosphates, that turn hydrophobic into hydrophilic areas. Therefore, the ImageJ analysis is done in a central area of each droplet and images are concatenated to measure the same area of the droplet to compare the fluorescence intensity of a specific area. Mean gray values and integrated density measurements are used to evaluate the fluorescence intensity of each droplet, having at least five regions are measured and averaged. As it is usual in qLAMP assays, increments in fluorescence intensity will be related to the amplification of dsDNA due to the Evagreen in solution that binds to the formed dsDNA.

Data analysis and filtering techniques

For every drain current measurement each sensor in the array is interrogated 5 times. The reported value is the average of the 5 measurements and the standard deviation is considered experimental noise. This drain current information allows the computation of FET sensitivity and resolution. The pH sensitivity is obtained with the linear regression of the drain current to pH function and surface potential sensitivity can be obtained by correlating current response to equivalent threshold voltage changes *via* the sensor's *trans*-conductance $[S_{I_{ds}} = g_m \times S_{V_g}]$.[42] The resolution is estimated by dividing the measured experimental noise with the recorded sensitivity $[pH_{min} = \sigma/S]$.[37] This ratio would indicate the minimum pH change that is electrically detectable with a particular FET.

The LAMP assays are optically and electrically monitored. The inclusion of EVA green into the reaction mix enables the standard fluorescent confirmation of DNA amplification products typically used for qPCR, while pH changes related to nucleotide incorporation are electrically monitored with the BioFETs. Increments in the fluorescence intensity are related to a greater concentration of dsDNA and reflect successful amplification of the target gene. Fluorescence images of the chip are analyzed using ImageJ (http://www.rsb.info.nih.gov/ij/) to estimate intensity with mean grey values. Increments in the recorded mean grey value indicate successful replication of target DNA and are computed as relative fluorescence changes. In addition, the results section presents differential images that result from the subtraction of before and after pictures. This subtraction is performed with the image calculator tools of ImageJ to highlight intensity differences caused by amplified dsDNA. These fluorescence images are controls for electrical measurements of DNA amplification reactions. LAMP-triggered pH changes are observed by comparing the measured drain current in monitoring DG-BioFETs before and after the reaction takes place inside the micro-chambers. Matlab scripts let the user select the micro-chamber to be analyzed, create histograms, and obtain other statistical metrics of the recorded current in the selected chamber. For a pixel-normalized evaluation, the drain current matrices before and after the reaction are subtracted creating a differential matrix that describe current and potential changes that occurred during amplification.

It will be discussed in the results section how acquired electrical measurements do not have significant signal-to-noise ratio. However, given that thousands of DG-BioFETs are monitoring a single reaction, the collected drain current data sets can be filtered with two techniques to improve the quality of the recorded signals. First, the pH resolution of DG-BioFETs is used as the performance metric to accept or reject individual sensors.[43] FETs with poor sensitivity or large noise can be identified with a resolution metric that is used to discard underperforming devices in the array and improve the quality of the collected data. Second, the Grubbs test and its iterative form of the Extreme Studentized Test (ESD) is used to detect and eliminate elements outside the expected normal distribution with a technique that has been previously used to filter data from sensor arrays or networks.[44,45] The collected data is filtered with algorithms that discard points outside the drain current normal distribution to enhance differences between current distributions in the reaction chambers and obtain clear signals of amplification. End-point LAMP reactions have a binary distribution of amplification *vs.* no-amplification, but the measurements collected from sensors have a highly normal distribution that can be subject to ESD elimination tests. The performance filter is set to have a threshold of maximum resolution of 0.5 pH units while the ESD test is done with probability threshold 'α' of 0.05 and a maximum number of iterations 'r' equivalent to half of the total number of points in the data set ($N/2$).

Results and discussion

Chip electrical characterization

Fig. 2 presents transfer characteristics for fluid and bottom gates of DG-BioFETs in the sensing array. It presents typical FET *I–V* curves, a 3D map of measured drain currents as a function of gate voltage, and drain current color coded maps of the 1024×1024 array. Fig. 2(a) shows how the full array responds to changes in the bottom gate potential while Fig. 2(d) shows that only sensors in the bottom of the reaction chambers respond to the fluid-gate bias that is established with the gold-coated silicon. The gold-coated wells significantly simplify electrolyte biasing inside the wells. Instead of having on-chip micro-reference electrodes for each well that can be difficult to pattern and connect or long electrodes without wells in contact with each droplet, a single node references all wells in the array simplifying the cost and operation of the experimental setup. Our attempts to use on-chip electrodes demonstrated that this strategy is expensive, diminish the performance of the devices, and reduces de volume and density of reactions (Fig. S2†). Hence, the gold-coated wells provide a simple solution to micro-droplet referencing in our array while confining the reaction. A

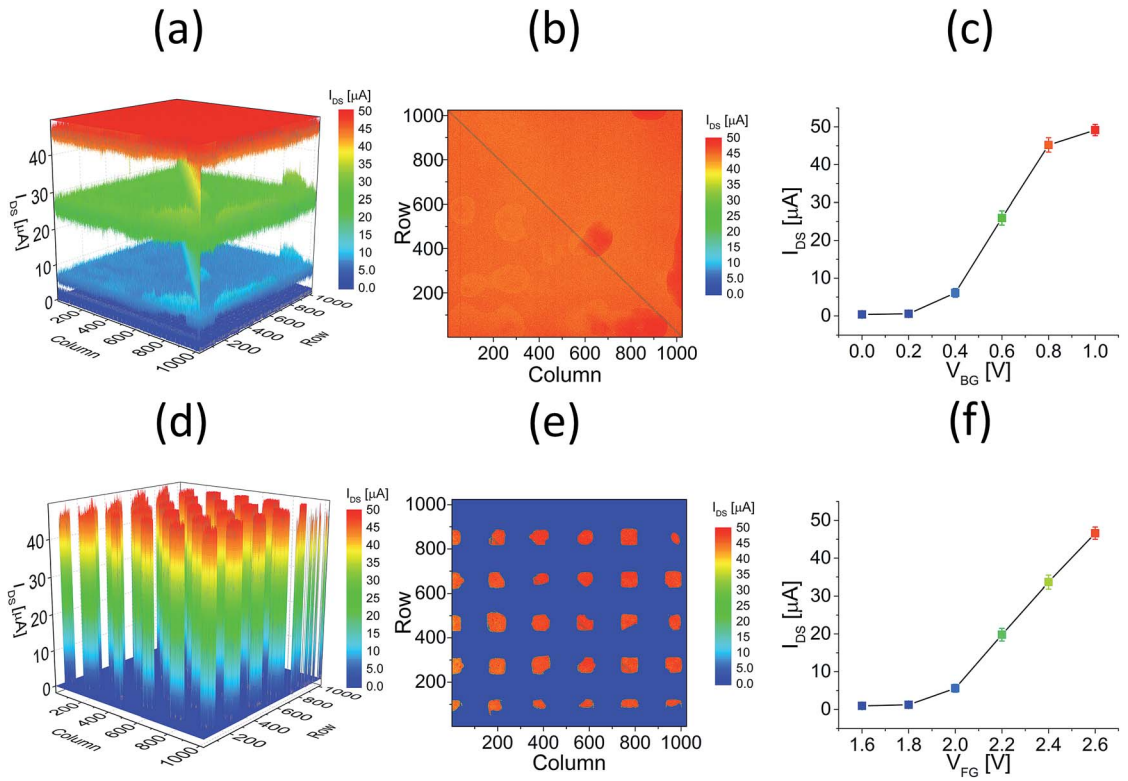

Fig. 2 Electrical characterization of the DG-BioFET array with gold-coated micro-chambers. (a) 3D plot showing the drain current as a function of the bottom gate bias. (b) Color coded map of the drain current in the array with $V_{BG} = 0.8$ V. (c) I–V transfer curve for the bottom gate. (d) 3D plot of the drain current as a function of the fluid-gate potential applied with the gold pseudo-reference electrode. (e) Color coded map of drain current in the array with $V_{FG} = 2.6$ V. (f) I–V transfer curve for the fluid-gate.

different perspective of the DG-BioFET electrical performance with the gold-coated chambers bonded to the sensing area is presented in the heat-maps of Fig. 2(b) and (e) that color code the current in each sensor. In Fig. 2(b) the position of reaction chambers has a correlation to the measured drain current controlled by the bottom gate. Even though the bottom gate is at the other side of the active silicon (Fig. S1†) charge coupling between gates in DG-BioFETs explain sensitivity of the bottom gate to elements in the surface. However this effect has no significant influence on pH monitoring and does not affect the electrical detection of LAMP reactions.[46] This same panel shows a diagonal (from top left to bottom right) of FETs with zero current that is used to assure the correct operation of the array's decoding circuit. Fig. 2(e) on the other hand presents a clear shape of each reaction chamber's bottom (the irregular shapes are related to PDMS reflow during the bonding step). Only BioFETs exposed to the electrolyte are affected by the fluid-gate potential resulting in the sectioned heat map with most of the transistors in the array having negligible current. Sensors with zero current are under the PDMS bonding layer and do not feel the fluid potential. Finally, Fig. 2(c) and (f) present standard I_{DS}–V_G plots for the bottom and fluid gates. These are typical FET transfer curves that show how the bottom gate has a lower threshold voltage and also an apparent current saturation with large V_{BG}. Lower and more uniform bottom gate threshold voltages have been reported for similar devices due to better control of the fabrication processes in the MOS gates.[36] Also, the drain current saturation (and the resulting lack of linearity in the bottom gate transfer curve) is caused by protection circuits in the PXI reading card that truncate high currents. The full sequence of heat maps for the multiple biasing conditions of Fig. 2 are presented in Fig. S5.†

pH sensitivity

More acidic electrolytes cause the protonation of the hafnium oxide layer, increasing the surface potential, and in consequence augmenting the NMOS transistor drain current. That trend is observed in Fig. 3(a) that shows how I_{DS} decreases with pH increments. Data presented in Fig. 3(a) is the average of all the transistors that are exposed to fluid in the array and the error bars represent the standard deviations across all the devices. This error reflects spatial variations across the chip that can be reduced by normalizing measurements of individual sensors. An independent transistor pH sensitivity analysis is presented in Fig. 3(b) that shows a color coded map of the surface potential as a function of pH. A similar plot is presented in Fig. 3(d) that presents the sensor estimated resolution that relates sensitivity and noise for each device. Sensors that are not in contact with fluid, and therefore not affected by the fluid-gate, have no sensitivity to pH changes and therefore an infinite resolution that is truncated at value of 1 for visualization

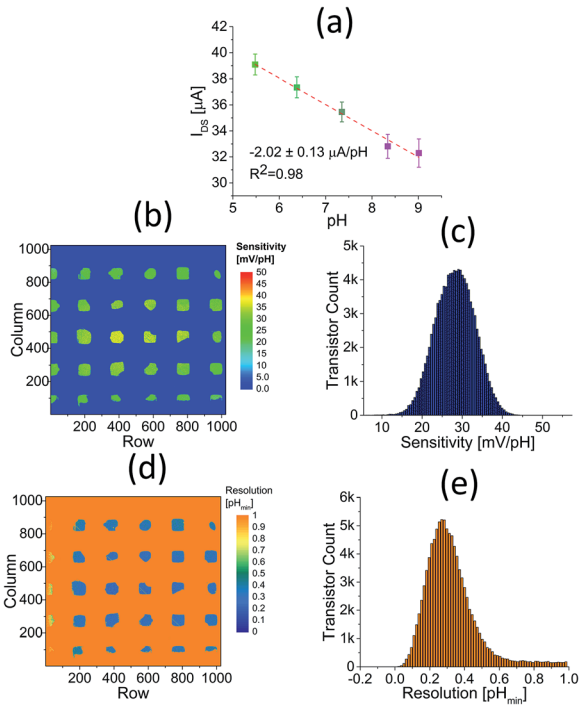

Fig. 3 pH sensitivity of DG-BioFET array. (a) Drain current as a function of electrolyte pH. (b) Color coded map of individual BioFET pH sensitivity. (c) Distribution of pH sensitivities. (d) Color coded map of resolution for each BioFET sensor. (e) Distribution of pH resolutions.

purposes. Histograms of both sensitivity and resolution of sensing BioFETs are presented in Fig. 3(c) and (e). The sensitivity histogram shows a normal distribution slightly skewed to the left with a mean sensitivity of 32 ± 4.9 mV pH^{-1}. This distribution is skewed because some sensors have a decreased response due to variable conditions in the sensing layer but have a rigid upper limit set by the Nernst relation. The measured sensitivity is far from the ideal Nernst limit but this low response is caused by the variable potential induced in the gold–electrolyte interface that is used as pseudo-reference electrode. Unlike standard Ag/AgCl reference electrodes, the gold surface has a small but significant reactivity to bulk pH changes that will decrease the FET sensitivity.[37] On the other hand, the resolution mean is of 0.51 ± 0.13 pH units with a normal distribution this time skewed to the right. This behavior is explained by the inverse relation between sensitivity and resolution that translates poor sensitivities into a high pH resolution.

Sensitivity and resolution in the array have coefficients of variation of 13% and 24% respectively. Even though these variations are significant, they do not affect the outcome of the amplification detection. First, the amplitude of the expected signals is larger from the variations between sensors. Second, the DG-BioFET platform enables a normalized pixel-to-pixel analysis precluding any false reading due to variations. Third, as it will be discussed in a later section, the analysis of the reaction is done with filtering techniques of the million different data points collected, allowing the elimination of outlying elements that cause the high variations.

Detection of pH changes in the DG-BioFET array is demonstrated in Fig. 4 that shows a drain current map of the array when chambers grouped in rows have different pH values. From top to bottom rows in the array, increasing pH values are correlated with lower currents. Quantification of the drain current recorded for each group of wells is presented in Fig. 4(b) and their current distributions are shown in Fig. S6.† The drain current to pH relationship shows a similar slope to the one obtained for the full chip experiments of Fig. 3 with a linear regression that indicates a pH sensitivity of ~2 μA pH^{-1}. Error bars in Fig. 4(b) represent variations between the thousands of DG-BioFETs in each group of chambers. These results demonstrate that it is possible to identify electrolytes of different pH value within the array by tracking the associated drain current of sensors in each chamber and biasing simultaneously with the gold-coated chambers. The ability to monitor the pH in each micro-chamber with the FET array will be used to detect the DNA amplification reactions.

Detection of LAMP reactions on DG-BioFET platform

We divided chambers in the array in positive and negative LAMP assays to test the electrical detection of the reaction. To evaluate the ability of the DG-BioFET array to detect the proton byproducts originated from LAMP reactions, chambers in the top half have full reactions while chambers in the bottom half have reactions without template DNA. No amplification and no pH change is expected from control chambers without template (negatives) while amplification is anticipated in the chambers with full (positive) reactions. Fig. 5 shows fluorescence and drain current measurements before and after the amplification reaction of *E. coli*'s eae gene with a template concentration of 85 ng μL^{-1}. Fluorescence increments are used as optical confirmation of DNA amplification by including intercalating dyes in the reaction mix. These reporters will bind to dsDNA and increase its fluorescence output[47] but do not affect the electrical measurement because they are outside the electrolyte's Debye length. The LAMP reactions are conducted in a reaction mix with an estimated equivalent salt concentration of 100 mM that has a Debye length of less than 1 nm.[48] While ions in solution are capable of interacting directly with the sensing layer, larger molecules outside the Debye length

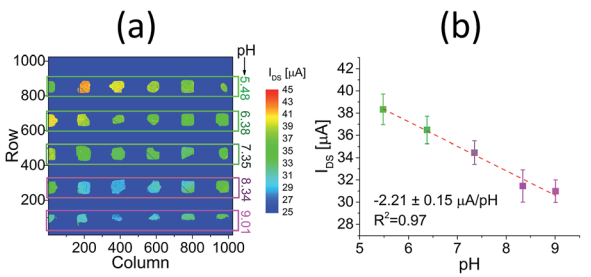

Fig. 4 Parallel pH measurements on the DG-BioFET array. (a) Color coded current map of the fluid-gate biased BioFET array with electrolytes of different pH in the micro-chambers and grouped in rows. (b) Quantification of drain current as a function of the electrolyte's pH in the micro-chambers.

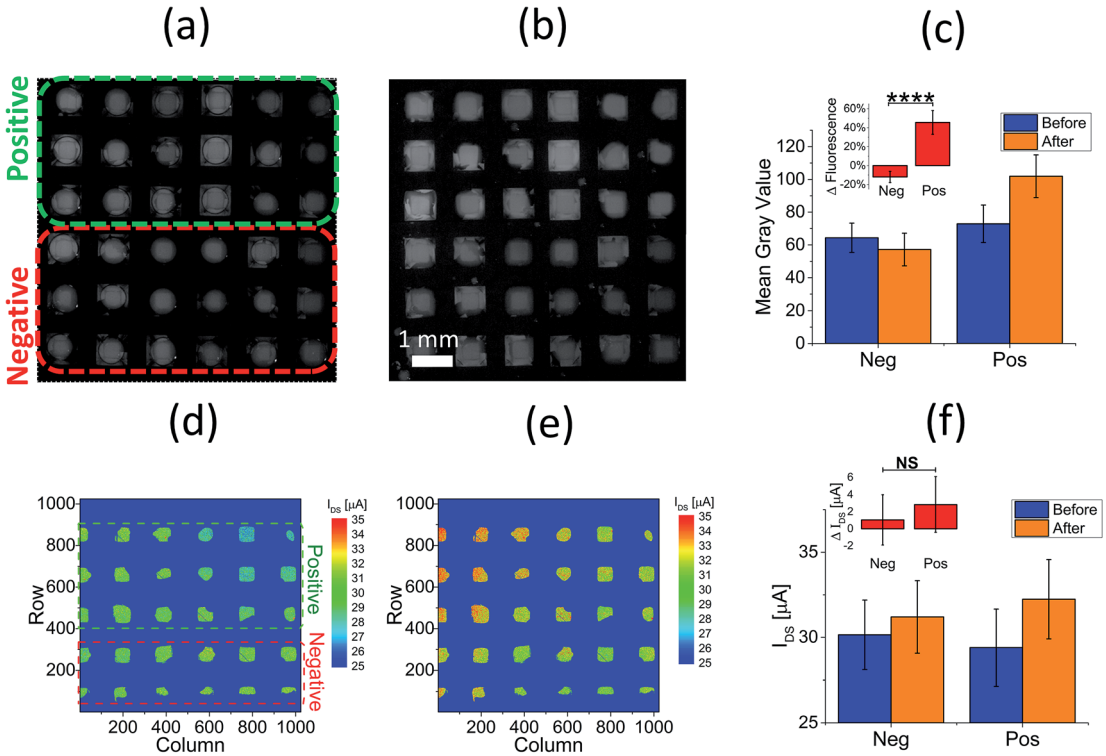

Fig. 5 Optical and electrical measurements before and after DNA amplification in a chip of 36 wells with positive and negative reactions. (a) Fluorescence image before DNA amplification, grouping positive and negative chambers. (b) Fluorescence image after the reaction. (c) Fluorescence intensity quantification for positive and negative samples. (d) Drain current map before DNA amplification. (e) Drain Current map after the amplification reaction. (f) Quantification of drain current measurements for FETs monitoring positive and negative reactions.

(including the fluorophores used for fluorescent confirmation) will not affect the BioFET response. In addition, other molecules present in solution that could be within the Debye length of the electrolyte, such as free dNTPs or buffering agents, do not have a net charge and therefore do not affect the surface potential of the BioFET. Without a net charge, non-specific absorption of other biomolecules has a negligible effect over the threshold voltage and hence no related current changes.

The chip status before the amplification occurs is reported in Fig. 5(a) and (d). Fig. 5(a) shows the fluorescence image of the full array before the reaction has taken place, with 36 chambers prepared with methods described previously. It also delineates the division between positive and negative samples. Even before the amplification takes place there are small differences between the fluorescence output of positive and negative reactions. These differences result from the DNA template that is present in the positive samples but has been replaced with water in the negative wells. The same array is also presented in Fig. 5(d), which instead of optical information shows the drain current of sensors in the bottom of the reaction chambers. Fig. 5(d) also shows the division between positive and negative samples but this electrical map is missing one row of negative reactions that are outside the DG-BioFET sensing area. Uncured PDMS between gold-coated chambers and the DG-BioFET array creates a good seal to hold the reactions during amplification but requires a difficult single attempt alignment because PDMS residues compromise the FET sensitivity once it touches the sensing area. Misalignments during the bonding process can leave chambers outside the sensing region reducing the number of chambers monitored by transistors.

The post-reaction measurements, presented in Fig. 5(b) and (e), were taken after the chip is heated for 60 min at 60 °C. The fluorescence image after amplification shows intensity increments for the positive samples and a lower intensity in negative samples. Multiplied dsDNA in positive reactions increase the number of binding points for the intercalating dye increasing the fluorescence output, while lack of amplification and partial photo-bleach of fluorescent molecules result in lower intensities in negative chambers. Even though we take great precautions to prevent photo-bleaching of the dye, the on-chip amplification protocol forces us to expose the droplets to microscope light when micro-injection capillaries or biasing micro-manipulator are aligned with the gold wells. Light exposure, in conjunction with the metallic surface, bleaches the fluorescent molecules and reduce their output in wells without amplification. Additionally, droplets in the micro-chambers change shape and have variable intensities after the reaction. These are effects of the amplification process that expand droplets, coat the surface of the chamber with byproducts, changing the interaction between the solution and the surface of the dielectric and the pseudo-reference electrode. However, the effects of slight differences in the starting fluorescence and

partial photo-bleach during amplification do not affect the amplification assessment. The amplification is observed as differences in the recorded fluorescence. Then, the discrete (per well) analysis will still accurately demonstrate the replication of DNA and serves as confirmation of the electrical assessment presented in Fig. 5(e). The 'after' electrical measurement reveals that in both positive and negative samples the drain current increased. However, increments in the positive chambers are higher by ~1.8 μA when compared to the ones in the negative samples. This differential analysis indicates that despite general variations across the chip related to drift and common noise, the sensors are detecting changes caused by the DNA amplification reactions.

The reported reaction time of 60 min may be adjusted as a function of the pathogen concentration. Assays that target a lower limit of detection may select longer amplification times while assays were the suspected pathogen is in high concentrations may reduce the amplification time. This amplification time is the limiting factor in the overall analysis time. The testing setup collects the electrical measurement in around 90 s and the reaction setup varies between 5–10 min. Therefore the overall time to detection is dominated by the reaction time. However, a full sample-to-result time estimation may also require the consideration of enrichment, concentration, or other sample preparation stages that could dominate the overall analysis time length.

Comparative fluorescence and electrical quantification are presented in Fig. 5(c) and (f). Insets in these panels quantify differential signals obtained from the two groups also describing the *P*-value significance level. Whereas the fluorescence increment in positive reaction chambers clearly differentiates amplification, the signal is more obscure in the electrical measurements where standard deviations are higher and means are closer. To have objective analysis of the output we performed *t*-tests of the two data sets to evaluate differences. The fluorescence signal between positive and negative reactions is clear, with a *P* value lower than 0.0001. However, the *t*-test of the electrical measurements results in a *P* value of 0.17 and therefore not statistically significant differences.

From the positive and negative assays, we demonstrate two important features of the electrical monitoring of the LAMP reactions. First, all the BioFET sensors, including those in reactions chambers with no amplification, presented current changes. This is the result of transistor drift, change in electrolyte referencing conditions, and common potentiometric changes during the reaction.[49] The common noise affecting all devices will require differential measurements that subtract the variations from control FETs. For example, unintended electrical signals resulting from non-specific absorption of biomolecules would be eliminated in the differential measurement that subtract these sources of common noise. Second, the current of DG-BioFETs monitoring a single reaction has high variability. The distributions of threshold voltages, pH sensitivities, and defects in the sensing membrane have an important effect over the measured drain current. To address those variations, we can use redundant measurements from the thousands of transistors available in our platform to obtain the highest possible signal-to-noise ratio for a robust differentiation of the LAMP byproducts. The employment of filtering techniques that detect and discard sensors with abnormal behaviors or the use of multiple sensors to reduce the standard deviation of a measurement, are techniques used in the past to reduce noise and facilitate the detection of LAMP-related signals. Both of these issues, common noise and measurement variations can be addressed with our 1024×1024 array. With a million devices and multiple reaction chambers we are able to dedicate chambers for negative controls for the rejection of common noise and drift. Also, in each chamber an average of 3500 sensors monitor the reaction. The large number of sensors allows the incorporation of the redundancy and filtering techniques that are required to improve the signal-to-noise ratio and enable statistically significant differentiation between positive and negative samples.

Performance and statistical filtering techniques

While the differential measurements are easy to perform, by simply subtracting the signal from negative controls to the sensing devices, the reduction of the measurement standard deviation is more challenging. In this section we present two methods that allowed us to improve the distributions of the recorded measurement to obtain statistically significant differences between positive and negative electrical measurements.

The first filtering approach targets to eliminate sensors that are not performing correctly. Our fabrication processes are in an experimental stage and certain steps, in particular the hafnium oxide deposition, have tolerances that will affect the device performance. Then, a resolution-based filter is used to reject sensors with poor response to pH or large noise. The calculated resolution combines the pH sensitivity and stability of the DG-BioFET creating a comprehensive evaluation parameter. Fig. 6(a) shows the DG-BioFET drain current difference matrix, calculated by subtracting after and before measurements of the experiment presented in Fig. 5. The sequence of images in Fig. 6(c) zooms at a reaction chamber and presents the same difference map but with pink pixels representing rejected BioFETs that have a poor resolution above a defined threshold. Plots of the rejected sensors in the full array are presented in Fig. S7.† Maps in Fig. 6(c) and S7† show that most of the sensors monitoring reactions in the array have a resolution better than 0.5, however as the performance metric is stricter (0.4 to 0.1 pH_{min}) the number of accepted sensors decreases and a resolution threshold of 0.1 would discard ~98% of the DG-BioFETs. The discarded sensors tend to be clustered in specific regions of the array. As it can be inferred from Fig. 3(d) and S7,† most of the discarded sensors in this experiment where located in the left of the array. This indicates that there is a correlation between the sensor performance and its position, suggesting spatial fabrication variations in the sensing membrane or the reading circuitry. The relation between the selected resolution threshold and the number of accepted sensors monitoring the reaction is presented in Fig. 6(b), which summarizes our first filtering technique based on individual sensor performance.

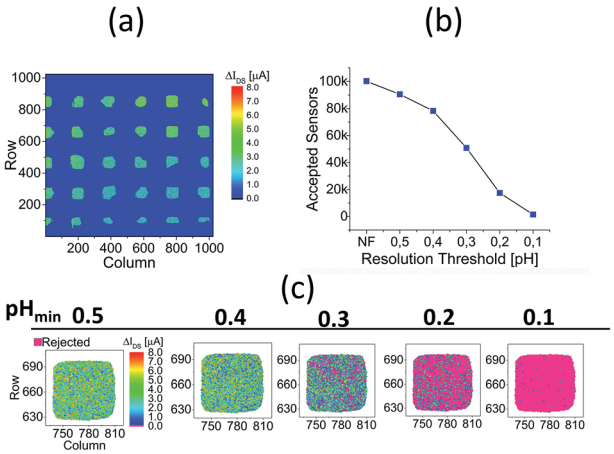

Fig. 6 Resolution based performance filtering. (a) Differential drain current matrix (after–before reaction) for negative and positive reactions. (b) Number of transistors with acceptable resolution as a function of the resolution threshold. (c) Sequence of eliminated FETs (rejected shown in pink) inside a reaction chamber as a function of a maximum threshold.

A second filtering strategy uses statistical analysis to detect abnormal elements. The Grubbs test is an algorithm that is used evaluate whether or not a data point falls out of a normal distribution.[45] It involves the identification of elements maximum distance to the mean, an estimation of a related t-distribution, and evaluation of a critical value that takes into account a user-defined rejection probability. The same process can be iterated over a data set with the extreme studentized deviate (ESD) test, eliminating unrepresentative elements in the array that fall outside the expected normal distribution. It is possible to use this elimination algorithm to our measurements because even though end-point LAMP provides a binary distribution (amplification *vs.* no amplification), the elimination of points is applied to the drain current measurements from the BioFETs which have a highly normal distribution. The elimination process is described in Fig. 7, which summarizes the outlier detection and elimination process in a flow diagram. To demonstrate the effect of applying the ESD technique into a recorded drain current data set, Fig. 8(a) and (b) present original and ESD filtered drain current distributions. The full data set in Fig. 8(a) presents a normal distribution skewed to lower current. After applying the ESD algorithm with $\alpha = 0.05$ and $r = N/2$, the current distribution is changed to the one presented in Fig. 8(b). Under those parameters around 20% of the sensors (8000 out of original 45 000) are discarded because they have a current value outside the expected normal distribution. This process statistically reduces variability (the standard deviation of the distribution is reduced by half) facilitating the identification of signals that are related by the DNA amplification reaction. The effect of the ESD technique on our amplification analysis is presented in Fig. 8(c) that shows the current differentials in positive and negative wells. The error bars in this plot represent the standard deviation between all sensors in each group. Before the ESD algorithm is applied to the collected data, large standard deviations resulting in non-

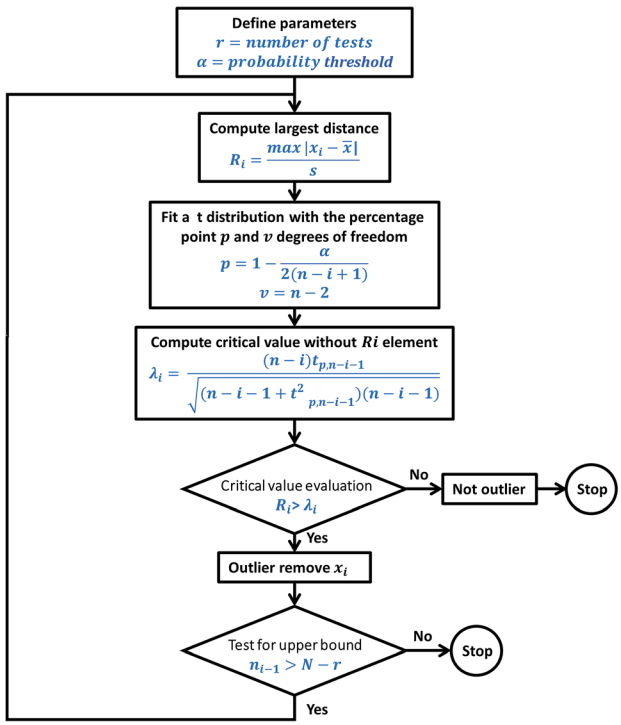

Fig. 7 Flow diagram of the ESD algorithm to detect and discard elements outside the normal distribution of the drain current measurements.

statistically significant differences between the two groups. However, after the data is filtered with the described algorithms that identify and eliminate measurements outside the normal distribution, the standard deviations of the measurements decrease and the *t*-test analysis confirm that the pH changes triggered by the amplification reaction create a significant

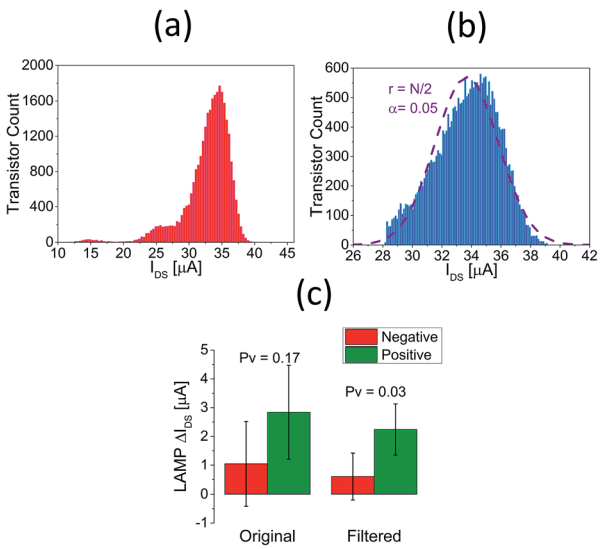

Fig. 8 Results of ESD elimination on electrical measurements of positive and negative reactions. (a) Full collected drain current data (b) ESD filtered drain current data. (c) Current differential distributions for positive and negative samples before after d ESD test.

electrical signal in the transistors that monitor the positive reactions. By filtering data from BioFETs we have reduced the *P* value from 0.17 to 0.03 confirming quantitatively that the electrical current of LAMP positive and LAMP negative measurements are different.

The redundancy that provides our 1024×1024 DG-BioFET array in combination with performance and statistical filters results in enhanced pH sensing of amplification reactions in the chambers with an improved signal-to-noise ratio. The use of the described techniques results in narrower distributions with clear signals recovered from a noisy environment inherent to the BioFET sensors and the amplification protocols. These statistical processes can be easily performed with minimal computing power and could be incorporated into the standard detection protocols. Leveraging the massive parallelism of the DG-BioFET array to clearly identify electrical signals caused by biochemical events is a viable alternative to deal with noisy environments. The large number of devices in our array has enabled us to apply statistical analysis that result in robust quantitative conclusions not possible with smaller BioFET platforms.

Parallel detection of foodborne pathogens

Using the techniques described in previous sections (primer dehydration, electrical monitoring of the DG-BioFET current, and data filtering), we have performed assays that show the ability of the DG-BioFET platform to perform a parallel detection of foodborne pathogens. Fig. 9 presents results from an experiment where the DG-BioFET array was divided in three regions: a control region (in the top) that had no dried primers and it is used as reference sensors to subtract common noise in differential measurements, a second group that was prepared with primers to amplify the invA gene for *S. typhi* detection, and a third group with primers for the amplification of the eae gene of shiga-toxin producing *E. coli* (STEC). These primer sets and reaction components that are utilized in our chip have been previously developed and tested for different matrixes and conditions.[34,35] Our off-chip confirmations, performed in a Mastercycler® RealPlex2 thermo-cycler (Eppendorf), are presented with the standard curves of Fig. S8 and S9.† These off-chip results confirm the conclusions of the authors that developed the assays. The limit of detection of the LAMP assays in pure culture can be as low as a few (1–18) CFU per mL but will be higher for more complex samples. It also confirms that there is no non-specific amplification due to cross reactivity with other targets or primer dimerization. Our assays achieve similar results to the ones previously reported but the changes in buffering conditions affect the reaction velocity, represented by the longer threshold times that we observe for the different concentrations.

The LAMP reaction mix, containing template 36 ng μL^{-1} of DNA extracted from an overnight culture of *S. typhi*, was injected in all chambers after primer dehydration. The before and after reaction fluorescence images are summarized in Fig. 9(a) that shows the differential fluorescence quantification. The bar plot in Fig. 9(b) evaluates increments in fluorescence by calculating relative intensity changes and describes *P*-value significance between the three groups. Similarly, the before and after drain current maps are condensed in Fig. 9(c) that shows the difference between the two electrical measurements. It is important to note that Fig. 9(c) presents the collected electrical data without the filtering and analysis techniques that has been previously discussed to improve the SNR, and therefore it is not the final assessment. Fig. 9(d) presents the current distributions of the raw difference data for each group of chambers, without filtering. These current distributions show the expected bell curves for drain current measurements but also present a significant portion of abnormal measurements specially towards lower currents. Even though we observed the anticipated result of greater changes for the *S. typhi* group, because the LAMP primers found a matching template, the large variations that are observed in our measurements results in non-statistically significant results between samples. The bar plot inset in Fig. 9(d) shows that there are differences between invA and the other two groups, but the large standard deviations prevent quantitative comparisons. This result reveals the importance of having methods to improve the SNR and reduce variability. Then, Fig. 9(e) presents the same current difference heat map of Fig. 9(c) but this time showing in pink the sensors that are discarded with our filtering algorithms based on the resolution performance with a threshold of 0.5 pH and the ESD test with $\alpha = 0.05$ and $r = N/2$. This heat map shows that many of the sensors in the left of the array are outliers or underperforming devices, indicating that there is spatial performance distribution in our array affecting the collected measurements. After discarding sensors, new current distributions for each group are calculated and the results are presented in Fig. 9(f). The filters discard the outlier elements, clarify the measurements mean, and result in narrower distributions with lower variations. A quantification of the filtered measurement is presented on the inset of Fig. 9(f) that present a bar plot quantification with significance values. The comparison between Fig. 9(d) and (f) clearly demonstrate the importance of having multiple sensors monitoring the same reactions and the utilization of filtering methods to improve the collected signal. The large noise that is intrinsic to the FET biosensors and the LAMP protocol prevent robust and accurate electrical measurements of amplification with the BioFETs. However, these variations and noise can be managed by exploiting the large quantity of devices available in our platform to obtain accurate measurements based on the captured drain current distributions. In addition, the filtering methods that we have developed allow the standardization of the measurements to obtain statistical assessments of LAMP amplification. Therefore, the inability to obtain statistically significant measurements without a large number of devices and filtering techniques demonstrate the importance of robust dense sensing platforms and statistical analysis to successfully use FET sensors in biological assays.

The differential fluorescence images of Fig. 9(a) act as a gold-standard control and shows that only wells prepared with primers for the amplification of the invA gene ended up with a larger concentration of dsDNA. Only in this group of wells the

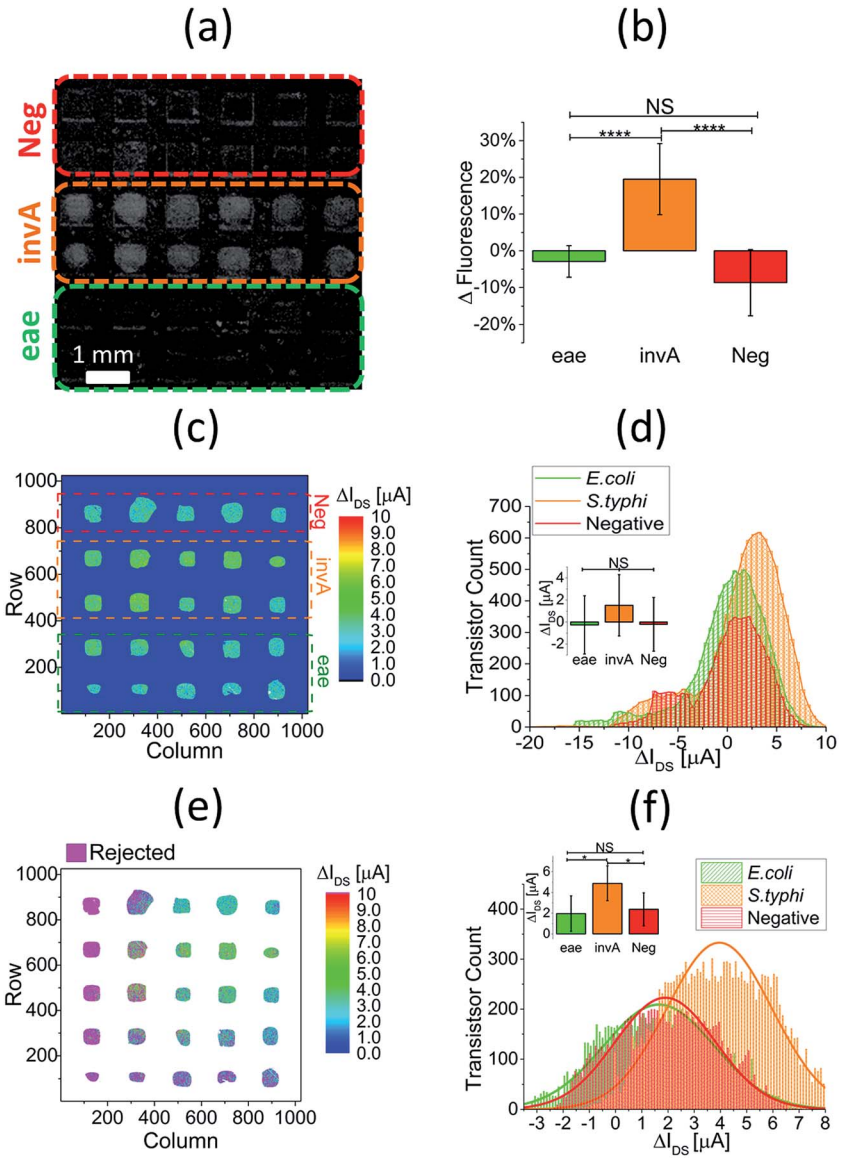

Fig. 9 Parallel detection of foodborne pathogens in DG-BioFET array chip. (a) Differential fluorescence image (after–before amplification) grouping reaction chambers based on the dried primer. (b) Quantification of relative fluorescence increments for each group of chambers. (c) Differential drain current map and groups of chambers with dried primers. (d) Unfiltered drain current distributions for the sensing BioFETs in each group of chambers. The inset bar plot quantifies mean, standard deviation, and statistical significance between data sets. (e) Differential drain current map with discarded sensors in pink and non-sensing devices (outside the wells) in white. (f) Filtered drain current distributions for each group of chambers. The inset bar plot shows mean, standard deviation and statistical significance between data groups.

template (*S. typhi*) finds a matching primer set that triggers the amplification reaction. On the other hand, the electrical difference map show changes in all reaction chambers but greater increments in chambers where amplification took place. This indicates that LAMP-induced pH changes affect the surface potential and the threshold voltage of the transistors of the invA group. The current differences are clear once the distributions are filtered with the techniques previously described. The quantitative analysis of filtered data indicate no difference (P value = 0.27) between wells with eae primer and negative controls, demonstrating that current changes in the wells prepared for *E. coli* detection are only common noise and not related to the amplification reaction. In comparison, the current from DG-BioFETs in reaction chambers with the invA primer is significantly different from the negative control (P value = 0.01) which indicates that the differential signal is related to the DNA amplification reaction that was fluorescently confirmed. The difference of drain currents of approximately 2.5 μA is expected given that the pH change in positive reactions oscillates between 0.8 and 1.2 pH units.[33] Results of a similar experiment where the injected template was not *S. typhi* but *E. coli* are presented in Fig. S10† demonstrating the two assays specificity and confirming the off-chip results. Additionally, these two experiments indicate that the detection performance is qualitative repeatable although there are differences in assay-to-assay electrical outputs. LAMP reliably amplifies DNA

whenever the primer set finds a matching template, generating the pH changes that triggers current changes in the BioFETs. However, the magnitude of the pH and current changes does variate between different assays. Therefore, threshold-based analysis normally (used in assays such as qPCR) need to be applied to the DG-BioFET platform to obviate output differences and have detection determinations based on calibrated thresholds. These parallel assays and the off-chip confirmations indicate that the LAMP protocol we use on our array only amplifies DNA when the dehydrated primer group finds a matching template. The same methods of primer dehydration and subsequent amplification and pH monitoring with DG-BioFETs could be expanded to crate panels of multiple relevant targets in the miniaturized system, following the successful trends of minimal hands-on work during detection assays.[50]

Sensitivity analysis

The sensitivity of the DG-BioFET array to LAMP reactions was evaluated by titrating the concentration of DNA template obtained from the bacterial cultures. For the assay presented in Fig. 10, all chambers were prepared with a single primer set for the detection of the eae gene of STECs. After the dehydration stage, a reaction mix with known template concentration was injected in each chamber. Chambers were grouped by rows, having the highest concentration of 9.13×10^8 CFU per mL in the bottom row (with an equivalent of 230 000 copies per reaction or 85 ng μL^{-1}), logarithmic dilutions in neighboring rows, and no template for the top row that acts as negative control. Fig. 10(a) shows the fluorescence differential image that results from subtracting 'after' and 'before' pictures. It shows a clear fluorescence increment in all reaction chambers with the exemption of the negative control. The relative fluorescence outputs for each group are quantified in Fig. 10(b) that show significant increases in the reaction chambers where amplification is expected but a small decrement in the control group. Furthermore, Fig. 10(b) shows that the reaction is able to replicate DNA when the template concentration is as low as 23 copies per reaction equivalent to 9×10^4 CFU per mL. Similar results were observed in the electrical measurements. Fig. 10(c) shows the differential drain current (after–before the reaction), and groups of chambers based on the concentration of the injected template DNA. In Fig. 10(d), changes of drain current in the BioFETs monitoring the reaction groups are quantified after applying the filtering strategies that have been described previously. These bar plots show that all DG-BioFETs presented current changes, but increments were higher in the chambers were the amplification reaction took place. The greater current increment in chambers with template are related to LAMP-triggered pH changes that do not occur in the control chambers.

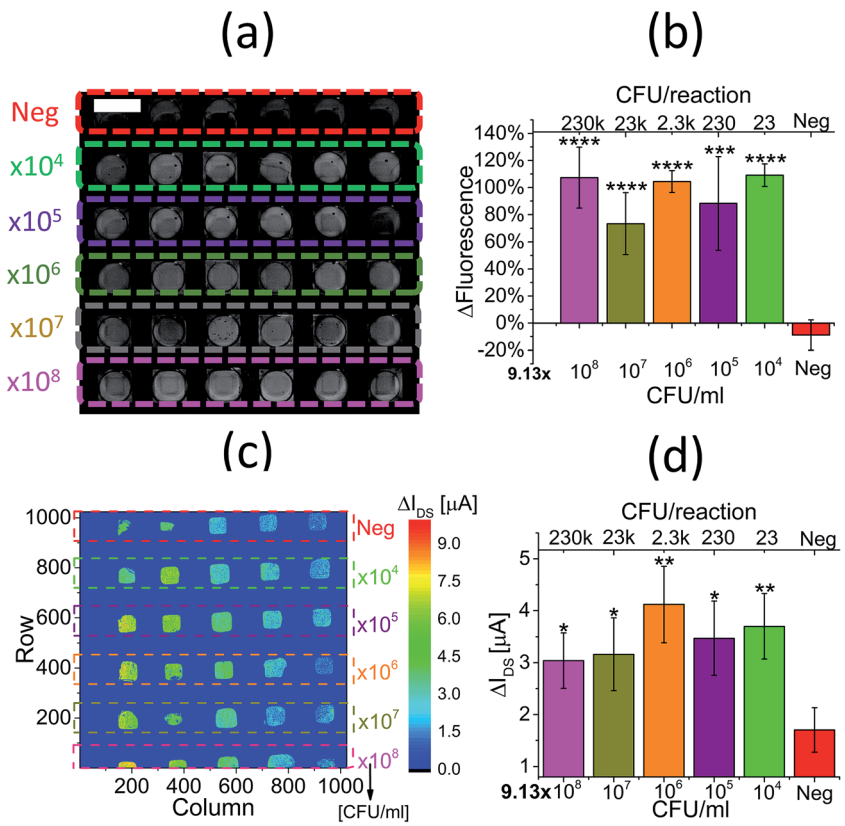

Fig. 10 Sensitivity evaluation of LAMP reaction on the DG-BioFET array that is divided in groups of chambers with different template concentration. (a) Differential fluorescence image (after–before amplification) and groups of reaction chambers with different DNA template concentration. (b) Quantification of fluorescence increments in each group. (c) Color coded map of the drain current difference of DG-BioFETs monitoring reactions. (d) Post-filtering quantification of drain current changes.

The quantifications presented as bar plots in Fig. 10 show that the magnitude of end-point fluorescence and drain current signals are independent from the starting concentration. This effect is explained by plateau stage of the amplification reactions that terminates LAMP regardless of the initial concentration. There are three main mechanisms behind the plateau stage of PCR and LAMP: the reactions run out of material to increase the number of amplicons, a very high concentration of created dsDNA prevents proper annealing of primers, or byproducts change the buffering conditions and impede the normal polymerase elongation.[51,52] For the case of pH-LAMP reactions, changes in the reaction mix composition that affect the polymerase behavior are likely to be the dominating cause of the plateau stage. In pH LAMP, the composition of the amplification reaction is modified by reducing the concentration of buffering agents to enhance the pH signals from the incorporation of nucleotides. The reduction of the buffer concentration facilitates electrical monitoring of the reaction but limits the ability of the polymerase to continue amplification when the byproducts change the reaction mix characteristics.[38] Under nominal conditions (*e.g.* 65 °C, 8.8 pH) the Bst polymerase incorporates 10 nmol of dNTP in 30 min, but if these conditions are changed the polymerase activity decreases and large variations will result in negligible activity causing the amplification stagnation.[53] With the minimized buffering conditions, the reaction's pH steps out of the working range faster than in regular reactions reaching the plateau stage due to polymerase inactivity. In Fig. 10, the plateau effect is evident both in the fluorescence and electrical measurements. Besides the saturation of current and fluorescence signals, another relevant result is a demonstrated electrical sensitivity of 23 copies per reaction. This limit of detection is too high for food safety applications. Therefore, our device can only be the sensing element of other more complex systems that are capable of increasing the number of microorganisms in the sample, either *via* growth or concentration,[20] and then performing the nucleic acid analysis. Additional optimization of the reaction composition and the preparation of the chambers with passivation agents such as silanes, can further reduce the limit of detection to a few copies per reaction chamber by limiting inhibitory effects present in small volumes[54] but constrains related to the volume in the reaction chambers will require preparatory stages prior amplification to achieve the desired LOD for food safety applications.

Conclusions

We have developed a DG-BioFET platform capable of on-chip electrical detection of multiple LAMP reactions in parallel. Our sensor array, which has an area of 7×7 mm^2 and over a million transistors, is divided in multiple independent reactions that are confined with simple but novel anisotropically etched gold-coated silicon micro-chambers. These wells act as both a common pseudo-reference electrode and reaction chambers, providing an effective solution to electrolyte biasing and augmenting the density of reactions in the array. Our characterization assays demonstrate that FET sensors have an average sensitivity of 32 mV pH^{-1} (equivalent to $\sim$2 μA pH^{-1}) with an estimated average resolution of 0.5 pH units. This pH sensing ability of the BioFETs was used to detect by-products of LAMP amplification reactions. The pH changes related to nucleotide incorporation[38] during LAMP are detected with the transistors in the form of drain current changes. We demonstrated how this sensing method can be complemented with a primer dehydration technique in our array for parallel detection of multiple genes in a single assay, demonstrating the pathway for screening assays based on BioFET devices.[32] With these techniques, thirty independent reactions were setup on our sensing array and monitored with fluorescent and electrical methods. As it was expected, in chambers with DNA amplification (where the dried primer group finds the target gene) the fluorescence intensity and drain current increased indicating greater concentrations of dsDNA and the generation of protons during elongation. The electrical signals are small and obscured by multiple noise sources, but the large quantity of individual DG-BioFETs that monitor each reaction in our platform allowed us to develop filtering methods to clearly identify LAMP-triggered surface potential changes. We demonstrate how the elimination of sensors in the array that are underperforming or are outside the expected normal distribution will reduce the measurement's standard deviation and create statistically significant differences between positive and negative samples, reducing the *P* value from an average of 0.17 to 0.03. These same methods can be applied to many Lab on a Chip assays that are difficult to analyze given the poor SNRs in multiple electrical biosensing platforms.

The DG-BioFET system and data analysis techniques that we developed were used for parallel foodborne pathogen detection experiments where *S. typhi* and *E. coli* are detected in a single assay. A differential current of $\sim$2.5 μA between sensors monitoring each group of reaction chambers reveal the specific DNA amplification reactions and also the power of arrayed reactions that can target multiple genes and use negative references to subtract common noise. Finally, we evaluated the sensitivity of the platform by titrating the concentration of template DNA. It was possible to detect concentrations of 23 copies per reaction, which represent an equivalent to 9.13×10^4 CFU per mL, but lower detection limits should be obtained with surface treatments and optimization of the reaction conditions that augment the efficiency of the reaction and eliminate inhibitory effects.

The current and upcoming challenges in food safety demand better pathogen detection tools that enhance the enforcing ability of regulatory agencies. Tighter food quality controls and faster outbreak reaction protocols are only possible with contamination sensors that sustain the performance of current methods but are portable, inexpensive, and easy to use. The platform that we have develop is aligned with these targets and miniaturize tools, minimize cost, and simplify detection of biological entities through DNA amplification. By combining sensitive molecular diagnosis techniques and semiconductor sensors we created a robust and simple platform that can be used for parallel bio-detection applications where screening assays are desired creating the core of a biosensing tool.

However, the success of this approach depends on novel sample preparation techniques. Even though LAMP has demonstrated to be more robust than other DNA amplification techniques and it can be performed with minimal sample preparation,[55] fully integrated detection systems for foodborne pathogens will require the incorporation of concentration,[56] partitioning,[57] and mixing devices.[58] Such integrated system that miniaturize and automate all processes for pathogen detection will promote screening tests in food samples and improve control over our food system.

Acknowledgements

This project was funded by the USDA-ARS through the Center for Food Safety Engineering at Purdue University and a subcontract 1935-42000-035 to the University of Illinois at Urbana-Champaign. We also acknowledge support from the NSF Center for Innovative Instrumentation Technology (NSF-CiiT) at the University of Illinois and Taiwan Semiconductor Manufacturing Company (TSMC) that provided wafers and technical advice.

References

1 P. Elizaquível, R. Aznar and G. Sánchez, *J. Appl. Microbiol.*, 2014, **116**, 1–13.
2 L. Cocolin, A. Rajkovic, K. Rantsiou and M. Uyttendaele, *Trends Food Sci. Technol.*, 2011, **22**, S30–S38.
3 A. B. Cronquist, R. K. Mody, R. Atkinson, J. Besser, M. T. D'Angelo, S. Hurd, T. Robinson, C. Nicholson and B. E. Mahon, *Clin. Infect. Dis.*, 2012, **54**, S432–S439.
4 P. M. Fratamico, J. L. Wasilenko, B. Garman, D. R. Demarco, S. Varkey, M. Jensen, K. Rhoden and G. Tice, *J. Food Prot.*, 2014, **77**, 180–188.
5 L. Hub, J. Holah and D. Napper, *Cleaning and disinfection practices in food processing*, Woodhead Publishing Limited, 2014, vol. 259.
6 H. K. Koh, *N. Engl. J. Med.*, 2010, **363**, 1653–1656.
7 R. L. Scharff, *J. Food Prot.*, 2012, **75**, 123–131.
8 B. Onyango, D. Miljkovic, W. Hallman, W. Nganje, S. Condry and C. Cuite, *Food recalls and food safety perceptions: the september 2006 spinach recall sace*, Fargo, ND, 2007.
9 R. Ivanek, Y. T. Gröhn, L. W. Tauer and M. Wiedmann, *Crit. Rev. Food Sci. Nutr.*, 2005, **44**, 513–523.
10 D. Rasko, D. Webster, J. Sahl, A. Bashir, N. Boisen, F. Scheutz, E. Paxinos, R. Sebra, C.-S. Chin, D. Iliopoulos, A. Klammer, P. Peluso, L. Lee, A. O. Kislyuk, J. Bullard, A. Kasarskis, S. Wang, J. Eid, D. Rank, J. Redman, S. Steyert, J. Frimodt, C. Struve, A. Petersen, K. A. Krogfelt, J. P. Nataro, E. Schadt and M. Waldor, *N. Engl. J. Med.*, 2011, **10**, 709–717.
11 L. Zach, M. E. Doyle, V. Bier and C. Czuprynski, *Food Control*, 2012, **27**, 153–162.
12 M. Ercsey-Ravasz, Z. Toroczkai, Z. Lakner and J. Baranyi, *PLoS One*, 2012, **7**, e37810.
13 E. C. D. Todd, *Meat Sci.*, 2004, **66**, 33–43.
14 J. Trienekens and P. Zuurbier, *Int. J. Prod. Econ.*, 2008, **113**, 107–122.
15 J.-Y. Yoon and B. Kim, *Sensors*, 2012, **12**, 10713–10741.
16 P. Ferrier and J. C. Buzby, *Food Control*, 2014, **38**, 227–234.
17 United States Food and Drug Administration, *Consum. Heal. Inf.*, 2010, pp. 1–3.
18 A. M. Foudeh, T. Fatanat Didar, T. Veres and M. Tabrizian, *Lab Chip*, 2012, **12**, 3249–3266.
19 L. Yang and R. Bashir, *Biotechnol. Adv.*, 2008, **26**, 135–150.
20 I.-H. Cho, A. D. Radadia, K. Farrokhzad, E. Ximenes, E. Bae, A. K. Singh, H. Oliver, M. Ladisch, A. Bhunia, B. Applegate, L. Mauer, R. Bashir and J. Irudayaraj, *Annu. Rev. Anal. Chem.*, 2014, **7**, 65–88.
21 I. H. Cho and J. Irudayaraj, *Anal. Bioanal. Chem.*, 2013, **405**, 3313–3319.
22 F. Yeni, S. Acar, Ö. G. Polat, Y. Soyer and H. Alpas, *Food Control*, 2014, **40**, 359–367.
23 R. D. Stedtfeld, D. M. Tourlousse, G. Seyrig, T. M. Stedtfeld, M. Kronlein, S. Price, F. Ahmad, E. Gulari, J. M. Tiedje and S. A. Hashsham, *Lab Chip*, 2012, **12**, 1454–1462.
24 S. N. Buss, A. Leber, K. Chapin, P. D. Fey, M. J. Bankowski, M. K. Jones, M. Rogatcheva, K. J. Kanack and K. M. Bourzac, *J. Clin. Microbiol.*, 2015, **53**, 915–925.
25 T.-H. Kim, J. Park, C.-J. Kim and Y.-K. Cho, *Anal. Chem.*, 2014, **86**, 3841–3848.
26 X. Zhi, M. Deng, H. Yang, G. Gao, K. Wang, H. Fu, Y. Zhang, D. Chen and D. Cui, *Biosens. Bioelectron.*, 2014, **54**, 372–377.
27 C. Guiducci and F. M. Spiga, *Nat. Methods*, 2013, **10**, 617–618.
28 C. A. Mack, *IEEE Trans. Semicond. Manuf.*, 2011, **24**, 202–207.
29 K.-I. Chen, B.-R. Li and Y.-T. Chen, *Nano Today*, 2011, **6**, 131–154.
30 B. Merriman, I. T. R&D Team and J. M. Rothberg, *Electrophoresis*, 2012, **33**, 3397–3417.
31 M. Kalofonou, P. Georgiou, C. P. Ou and C. Toumazou, *Sens. Actuators, B*, 2012, **161**, 156–162.
32 C. Duarte, E. Salm, B. Dorvel, B. Reddy and R. Bashir, *Biomed. Microdevices*, 2013, **15**, 821–830.
33 C. Toumazou, L. M. Shepherd, S. C. Reed, G. I. Chen, A. Patel, D. M. Garner, C.-J. Wang, C.-P. Ou, K. Amin-Desai, P. Athanasiou, H. Bai, I. M. Q. Brizido, B. Caldwell, D. Coomber-Alford, P. Georgiou, K. S. Jordan, J. C. Joyce, M. La Mura, D. Morley, S. Sathyavruthan, S. Temelso, R. E. Thomas and L. Zhang, *Nat. Methods*, 2013, **10**, 641–646.
34 F. Wang, L. Jiang and B. Ge, *J. Clin. Microbiol.*, 2012, **50**, 91–97.
35 S. Chen, F. Wang, J. C. Beaulieu, R. E. Stein and B. Ge, *Appl. Environ. Microbiol.*, 2011, **77**, 4008–4016.
36 C. Duarte-Guevara, F.-L. Lai, C.-W. Cheng, B. Reddy, E. Salm, V. Swaminathan, Y.-K. Tsui, H. C. Tuan, A. Kalnitsky, Y.-S. Liu and R. Bashir, *Anal. Chem.*, 2014, **86**, 8359–8367.
37 C. Duarte-Guevara, V. V. Swaminathan, M. Burgess, B. Reddy, E. Salm, Y.-S. Liu, J. Rodriguez-Lopez and R. Bashir, *Analyst*, 2015, **140**, 3630–3641.
38 E. Salm, Y. Zhong, B. Reddy Jr, C. Duarte-Guevara, V. Swaminathan, Y.-S. Liu and R. Bashir, *Anal. Chem.*, 2014, **86**, 6968–6975.

39 W. Sant, M. L. Pourciel, J. Launay, T. Do Conto, A. Martinez and P. Temple-Boyer, *Sens. Actuators, B*, 2003, **95**, 309–314.

40 W. Sant, P. Temple-Boyer, J. Launay and A. Martinez, *Sens. Actuators, B*, 2011, **160**, 59–64.

41 M. L. Pourciel-Gouzy, S. Assié-Souleille, L. Mazenq, J. Launay and P. Temple-Boyer, *Sens. Actuators, B*, 2008, **134**, 339–344.

42 A. Bandiziol, P. Palestri, F. Pittino, D. Esseni, L. Selmi and A. E. Model, *IEEE Trans. Electron Devices*, 2015, **62**, 3379–3386.

43 M. Zhang, *IEEE Transactions on Very Large Scale Integration Systems*, 2010, **18**, 171.

44 A. Kauffmann and W. Huber, *Genomics*, 2010, **95**, 138–142.

45 D. J. Cook, *IEEE Pervasive Computing Magazine*, 2007, **6**, 105–108.

46 M.-J. Spijkman, K. Myny, E. C. P. Smits, P. Heremans, P. W. M. Blom and D. M. de Leeuw, *Adv. Mater.*, 2011, **23**, 3231–3242.

47 F. Mao, W.-Y. Leung and X. Xin, *BMC Biotechnol.*, 2007, **7**, 76.

48 V. V. Swaminathan, P. Dak, B. Reddy, E. Salm, C. Duarte-Guevara, Y. Zhong, A. Fischer, Y. S. Liu, M. A. Alam and R. Bashir, *Appl. Phys. Lett.*, 2015, **106**, 1–5.

49 J. L. Chiang, S. S. Jan, J. C. Chou and Y. C. Chen, *Sens. Actuators, B*, 2001, **76**, 624–628.

50 P. Ruggiero, T. McMillen, Y. W. Tang and N. E. Babady, *J. Clin. Microbiol.*, 2014, **52**, 288–290.

51 P. Kainz, *Biochim. Biophys. Acta*, 2000, **1494**, 23–27.

52 K. Nagamine, K. Watanabe, K. Ohtsuka, T. Hase and T. Notomi, *Clin. Chem.*, 2001, **47**, 1742–1743.

53 C. Sandalli, K. Singh, M. J. Modak, A. Ketkar, S. Canakci, I. Demir and A. O. Belduz, *Appl. Microbiol. Biotechnol.*, 2009, **84**, 105–117.

54 R. Kodzius, K. Xiao, J. Wu, X. Yi, X. Gong, I. G. Foulds and W. Wen, *Sens. Actuators, B*, 2012, **161**, 349–358.

55 G. L. Damhorst, C. Duarte-Guevara, W. Chen, T. Ghonge, B. T. Cunningham and R. Bashir, *Engineering*, 2015, **1**, 324–335.

56 H. B. Vibbert, S. Ku, X. Li, X. Liu, E. Ximenes, T. Kreke, M. R. Ladisch, A. J. Deering and A. G. Gehring, *Biotechnol. Prog.*, 2015, 1–12.

57 C. Zhang, D. Xing and Y. Li, *Biotechnol. Adv.*, 2007, **25**, 483–514.

58 S. Hakenberg, M. Hügle, M. Weidmann, F. Hufert, G. Dame and G. A. Urban, *Lab Chip*, 2012, **12**, 4576.